FeOOH modified H-TiO_2 nanorods array for stable and improved low-bias photoelectrochemical water splitting

G. Panzeri[a], R. Dell'Oro[a], A. Panzeri[a], M. Sansotera[a], V. Russo[b], C. L. Bianchi[c], L. Magagnin[a,*]

[a] Department of Chemistry, Materials and Chemical Engineering Giulio Natta - Politecnico di Milano, Milano, Italy

[b] Department of Energy - Politecnico di Milano, Milano, Italy

[c] Department of Chemistry - Università degli Studi di Milano, Italy

* Corresponding author: luca.magagnin@polimi.it

Iron oxyhydroxide (FeOOH) was implemented as a low-cost, stable and earth-abundant catalyst on a hydrogenated titania nanorods array (H-TiO_2/FeOOH), for photoelectrochemical water splitting applications. The hydrogenation treatment was selected to enhance the maximum photocurrent density delivered by the titania photoanode (from 0.65 mA cm^{-2} to 1 mA cm^{-2} at +1.23 V vs RHE) while the implementation of FeOOH resulted in a significant improvement of the photoelectrochemical activity at low bias. The optimized photoelectrode showed ~0.6 mA cm^{-2} at +0.4 V vs RHE, with a saturation current of 1.05 mA cm^{-2}. Insights on the role of FeOOH were revealed by electrochemical impedance and photoluminescence measurements, suggesting a reduction of the charge transfer resistance at the electrolyte interface and lower recombination events. The reliability of the photoelectrode was measured in 1 M NaOH solution, with a 5 h test at 1.23 V vs RHE, under illumination (1 sun). A stable photocurrent was measured during the entire duration of the test, and the photoelectrochemical behavior remained unchanged.

KEYWORDS: photoanode, titania, hydrogenation, catalyst, earth-abundant

1 Introduction

Since the first demonstration of photoelectrochemical water splitting by Fujishima and Honda in 1972 [1], titania (TiO_2) has been extensively studied and it is considered one of the most promising photoanodes [2,3] because of its low cost and chemical/electrochemical stability in all pH range. Moreover, titania is also exploited for the decomposition of organic pollutants because of its high photocatalytic activity [4–6]. Despite these advantages, its large bandgap (~3.2 eV) limits the portion of the solar spectrum absorbed, resulting in lower photocurrents values if compared to other photoanode material e.g. $BiVO_4$ (2.4 eV), Fe_2O_3 (2.2 eV) [7–9]. To cope with these limitations, one-dimensional morphologies, such as nanotubes or nanorods, are typically exploited to increase light absorption and to improve the electrical pathway for the photogenerated charges.

Titania nanorods arrays can be obtained through hydrothermal synthesis, resulting in the formation of (101) oriented rutile rods thanks to the small lattice mismatch with FTO substrate [10]. Rutile crystal phase is characterized by a bandgap (3.0 eV) smaller than the anatase one (3.2 eV) [11], harvesting also part of the radiation in the lower wavelenght part of the visible spectrum ($\lambda \lesssim 413$ nm). Another strategy to increase the photogenerated charges consists in the doping of the TiO_2, achieved through the introduction of impurities atoms, such as transition metals and non-metals [12]. The chemically defected structure may result indeed in the improvement of the electrical properties, reducing the ohmic barrier and recombination events, or by introducing states between the conduction and valence bands. The latter would result in a reduction of the actual bandgap of the material, capable to absorb photons with larger wavelengths. A well-known doping process is the hydrogenation treatment which induces oxygen vacancies and surface hydrogenation, improving the absorption and the photocatalytic activity [13,14]. Wang *et al.* firstly demonstrated the effectiveness of annealing in a hydrogen-containing atmosphere of a TiO_2 nanorod array photoanode, showing a striking improvement in the photocurrent [15]. Moreover, the implementation of a catalytic material, aimed to enhance the charge transfer from the semiconductor surface to the electrolyte, is a consolidated strategy to improve the overall photoelectrochemical behavior [16]. However, only a few literature studies exploited this approach in the case of titania nanorods [17–22], while in the cases of $BiVO_4$ [23,24] and Fe_2O_3 [25,26], earth-abundant NiOOH and FeOOH catalysts [27] have been extensively investigated.

In this study, we photo-electrodeposited earth-abundant and low-cost FeOOH catalyst onto hydrogenated TiO_2 nanorods array. The combination of hydrogenation treatment with catalyst implementation enhanced the photoelectrochemical behavior showing a significant photocurrent increase also under a low-bias, which is particularly important in a hypothetical tandem configuration for bias-free water splitting [28–30]. The reliability of the FeOOH catalyst is demonstrated by testing the H-TiO_2/FeOOH photoelectrode in a strongly alkaline solution, suitable for the electrolysis process.

2 Experimental methods

2.1 TiO_2 hydrothermal synthesis

Fluorine doped Tin Oxide (FTO) coated glass (Aldrich, 300 mm x 300 mm x 2.2 mm, surface resistivity 7 Ω/sq) was used as a substrate. The FTO was sonicated for 20 min in a 1:1:1 vol. mixture of deionized water, acetone (Sigma-Aldrich, purity 99%), and propanol (Sigma-Aldrich, purity 99.5%). A portion of FTO substrate was covered with PTFE tape to guarantee good electrical contact for the photoelectrode. The cleaned substrate was placed in a 100 ml Teflon-lined reactor, inclined against the wall with the conductive face facing up, filled with a solution composed of 20 ml of deionized water, 20 ml of hydrochloric acid (Sigma-Aldrich, purity 37.5%), and 0.67 ml of titanium n-butoxide (Aldrich, purity 97%), previously left under stirring for 15 minutes. The autoclave was placed in a laboratory oven and maintained at 150 °C for 5 hours, setting a heating ramp of 5 °C/min. The sample was removed from the autoclave and washed with copious amount water to remove all the possible remains of the synthesis solution from the nanorods array. Finally, the nanorods were annealed on a plate at 500 °C for 30 minutes in air atmosphere.

2.2 TiO_2 hydrogenation

Hydrogenation of TiO_2 nanorods was performed in a tubular furnace using a 3 cm diameter quartz tube. An 80 % v/v argon and 20 % v/v hydrogen atmosphere was obtained by fluxing 4 Nl h^{-1} of Ar and 1 Nl h^{-1} of H_2 in the vial, that was inserted directly in the furnace previously heated at 350 °C. After 30 min the vial was removed from the oven and let cool, after switching off the hydrogen flux.

2.3 FeOOH photo-electrodeposition

After hydrogenation, iron oxyhydroxide (FeOOH) catalyst was deposited by photoassisted electrodeposition in an aqueous solution containing 5-100 mM $FeSO_4 \cdot 7 H_2O$ (Sigma-Aldrich, purity 99 %). A freshly prepared solution was employed for every batch tested due to its limited time stability, since precipitation is likely to occur. The setup featured a three-electrode configuration with TiO_2 nanorods array as a working electrode (WE), a platinum-coated titanium net as a counter electrode (CE), and an Ag/AgCl (3M KCl) reference electrode (RE). The photo-electrodeposition was carried out at +0.25 V vs Ag/AgCl for 5 minutes with a potentiostat (AMEL 2559), under constant 100 mW cm^{-2} (AM 1.5 G) illumination using an ABET 83 SunLite solar simulator 11002, equipped with a 100 W Xenon arc lamp.

2.4 Materials characterization

XRD measurements were carried out with a Malvern Panalytical EMPYREAN diffractometer. The measurements were done in thin-film mode with $Ka1_{Cu}$=1.54058 Å. SEM micrographs were obtained using a ZEISS EVO 50 EP, equipped with an OXFORD INCA ENERGY 200 EDS unit. XPS measurements were performed with a M-Probe – Surface Science Instrument employing an un-monochromatized Al Kα source (photon energy = 1486.6 eV) at normal emission and room temperature. For high-resolution analysis, 1s level hydrocarbon-contaminant carbon was taken as the internal reference at 284.6 eV. Fittings were performed using pure Gaussian peaks, Shirley's baseline, and without any constraints. The photoelectrons were collected with a pass energy of 20 eV for high-resolution spectra and 40 eV for wide spectra. The overall FWHM resolution of the combined photon source and the spectrometer is below 1 eV. Micro-Raman and photoluminescence (PL) measurements were performed with a Renishaw In Via spectrometer equipped with an Ar^+ laser, λ = 514.5 nm, keeping the power on the sample below 1 mW. A quantitative evaluation of the amount of catalyst deposited was performed with inductively coupled plasma–optical emission spectrometry (ICP-OES) Perkin Elmer Optima 8300. The photoelectrochemical behavior was assessed through linear scan voltammetries (LSV) with a three-electrode cell including photoelectrode (WE), platinum net (CE), and Ag/AgCl (3M KCl) (RE) immersed in a 1 M NaOH solution (pH=13.6). The measurements were acquired with AMEL 2559 potentiostat setting 10 mV s^{-1} scan rate, under constant AM 1.5 G light radiation using an ABET 83 SunLite solar simulator 11002.

3 Results and discussion

3.1 TiO_2 nanorods array

The synthesis of a dense array of TiO_2 nanorods through hydrothermal process was optimized based on the previous literature works [10,15]. A homogenous coverage over a large area sample (3 x 4 cm^2) was obtained at a heating ramp of 5 °C min^{-1} and a reaction temperature of 150 °C (Fig 1a). SEM micrographs showed the characteristic tetragonal shape of TiO_2 nanorods, having diameters in the range of 100-200 nm and a length of about 1-1.5 µm (Fig 1b,c). The annealing conditions were selected according to literature data and the optimal parameters were defined based on the photoelectrochemical response (Figure S1-2). Air annealing at 500 °C greatly improved the photoelectrochemical behavior with respect to lower temperature treatments: a relatively short annealing time (30 min) was already effective in improving the semiconductor properties of the nanorods (Figure S1,2). The annealing step was fundamental to adjust the stoichiometry of the material and to improve the crystallinity of the rutile phase, whose diffraction peaks (36.1°, 41.3°, 62.9°) resulted to be well defined and sharp (Figure 1d). The relative intensities of the peaks indicated the preferential orientation of the nanorods along (101), in agreement with the SEM micrographs (Figure 1b-d). As a consequence, the open-circuit potential under illumination was shifted towards more negative potential values (0.2 V vs RHE) and the saturation current density reached ~0.65 mA cm^{-2} at 1.23 V vs RHE.

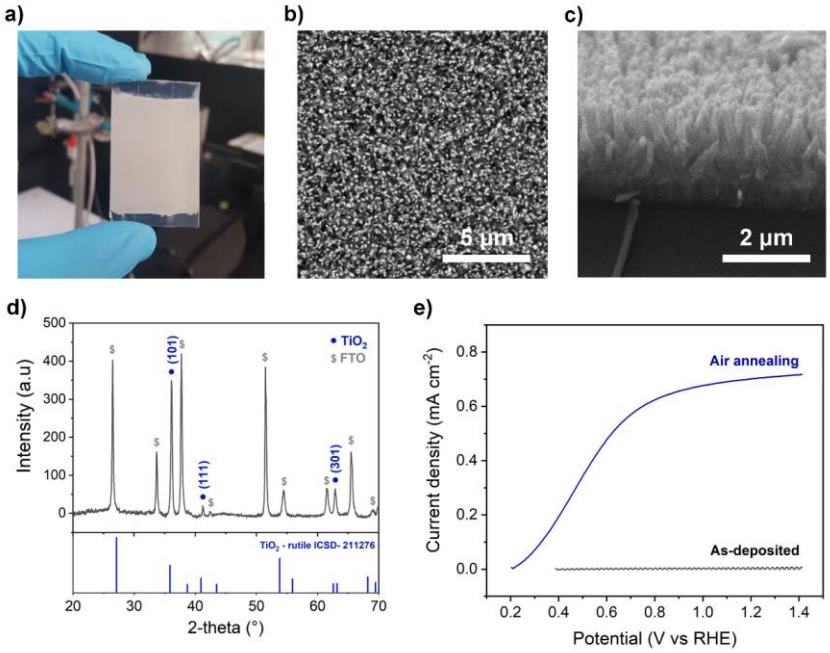

Figure 1 TiO_2 nanorods array (a) Real pic of the sample (b-c) SEM micrographs. (d) XRD spectrum of the TiO_2 after air annealing and pattern of the rutile phase. (e) Anodic linear sweep voltammetry of TiO_2 nanorods photoelectrode, before and after air annealing, under AM 1.5 G illumination [100 mW cm^{-2}] in 1 M NaOH solution.

3.2 Effect of hydrogenation

The hydrogenation treatment was introduced to improve the photoelectrochemical activity of the TiO_2 nanorods. The annealing in a reductive environment is expected to increase the density of oxygen vacancies [13,14], which have a critical role in determining the surface and electrical properties, such as light absorption, electrical conductivity, and charge transport. Different temperature conditions were tested in the 250-450°C range, with a reducing atmosphere composed of 20 % v/v H_2 and 80 % v/v Ar. The intermediate temperature (350°C) introduced an enhancement of the photoelectrical behavior of the TiO_2 nanorods, increasing the saturation photocurrent density to 1 mA cm^{-2} and improving the fill factor of the curve. Hydrogenation treatment to 250 °C was insufficient to produce a significative change, whereas the performances

dropped after the hydrogenation at 450 °C (Figure S6) probably due to an excessive introduction of oxygen vacancies in the material reducing its conductivity [15].

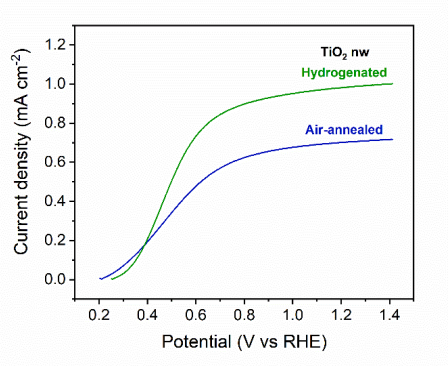

Figure 2 Anodic linear sweep voltammetry of TiO_2 nanorods photoelectrode, air annealed and hydrogenated, under AM 1.5 G illumination [100 mW cm^{-2}] in 1 M NaOH solution.

Raman and PL analysis was performed to investigate the modification induced by the annealing treatments. The Raman spectra of TiO_2 nanorods after hydrothermal synthesis, air annealing, and hydrogenation are reported in Figure 3a. They all show the peculiar features of rutile TiO_2, located at about 235 cm^{-1}, 445 cm^{-1}, and 611 cm^{-1} [31], confirming the XRD results previously described. The relative intensity of the two major peaks slightly changes after treatments, while their position and width remained unchanged, suggesting minor modifications in the rutile structure. Actually, the large peaks' characteristics of rutile TiO_2 substantially change only in presence of a high defectivity or strong confinement effect, in contrast to anatase phase whose very sharp Raman peaks shift or change in shape due to minor modification of the structure [31]. On the other hand, PL measurements (Figure 3b) revealed differences in the material before and after treatments: the as-synthesized nanorods showed a broad PL band in the red region of the visible (at about 1.8 eV), suggesting the presence of states within the energy gap due to defects and oxygen vacancies [32]. As expected, the PL signal was drastically reduced by the annealing treatment in air, which improved the sample crystallinity through rearrangement of the atoms and filling of the oxygen vacancies. Conversely, during hydrogenation, formation of acceptor-type defects and oxygen reduction is expected, resulting in states within the energy gap and a consequent intensification of the PL band.

Commentato [VR1]: Più generico, perché capire quali stati danno PL, soprattutto eccitando con il verde che è sotto il gap, non è così semplice (se ti interessa dai un'occhiata al paper che ti ho indicato come referenza per la PL)

Commentato [GP2R1]: Grazie mille

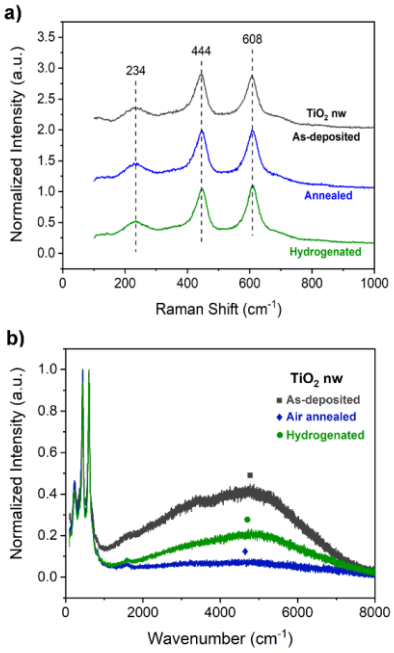

Figure 3 As-deposited, air annealed and hydrogenated TiO_2 nanorods (a) Raman spectrum. (b) photoluminescence spectrum.

Besides, XPS analysis of the air annealed and hydrogenated samples was performed at low binding energy, to obtain information on the position of the valence band. The presence of a band tail at about 0.3 eV agreed with the formation of acceptor-type defects within the bandgap, increasing the light absorption (Figure 4). This result is in agreement with the higher saturation photocurrent density observed in the photoelectrochemical characterization (Figure 2)

Commentato [VR3]: Come mai non hai fatto l'analisi per il campione as prepared?

Commentato [GP4R3]: Non abbiamo dato troppa importanza al campione as-prepared perché non mostraattività photoelettrochimica (Figure 1). Abbiamo scelto di fare XPS su i campioni più significativi a causa dell'accesso limitato allo strumento

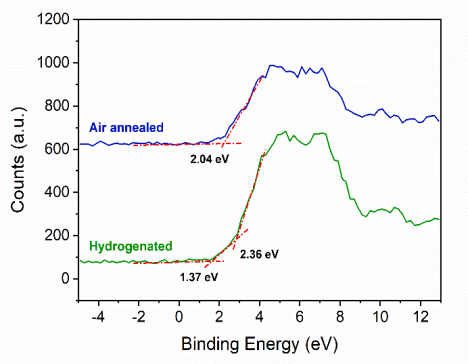

Figure 4 XPS valence band spectra of air annealed and hydrogenated TiO_2 nanorods.

3.3 FeOOH catalyst implementation

The iron oxyhydroxide (FeOOH) catalyst was deposited onto the H-TiO_2 nanorods through photo-electrodeposition at 0.25 V vs Ag/AgCl for 5 min using an iron sulfate solution. Both XRD and SEM analyses were unable to show any change in microstructure and morphology after the catalyst deposition, due to the small amount of deposited material. To determine the catalyst composition and elemental oxidation state, XPS was carried out (Figure 5a). High-resolution XPS analysis in the region of Ti *2p* peaks revealed that after catalyst deposition H-TiO_2 nanorods remained unaltered showing the typical double signal system of pure titanium dioxide with Ti $2p_{3/2}$ and Ti $2p_{1/2}$ at 458.5 and 464.2 eV (Figure 5b), respectively [17]. The region of O *1s* signals was also observed by high-resolution XPS analysis and H-TiO_2 nanorods showed a peak that can be fitted in two contributions (Figure 5c): one at 529.9 eV ascribable to oxygen as oxide and another at 531.6 eV due to hydroxyl groups [33]. Due to the deposition of the FeOOH catalyst, the characteristic region of Fe *2p* (Figure 5d) was also investigated and the peaks of Fe $2p_{3/2}$ and Fe $2p_{1/2}$ at around 711 and 724 eV were observed [34,35]. These signals are in the typical range of Fe^{3+} of iron oxyhydroxide and the broad shape of Fe $2p_{3/2}$ peak corresponded to the literature data on FeOOH [36–38]. FeOOH peaks are usually assigned as a single $2p_{3/2}$ and $2p_{1/2}$ system, even if two contributions in each signal can be distinguished: at 710.6 and 712.5 eV for Fe $2p_{3/2}$, and at 723.9 and 725.7 eV for Fe $2p_{1/2}$. The former can be ascribed to an electronic shift due to oxidic O; the latter to interactions with hydroxylic O.

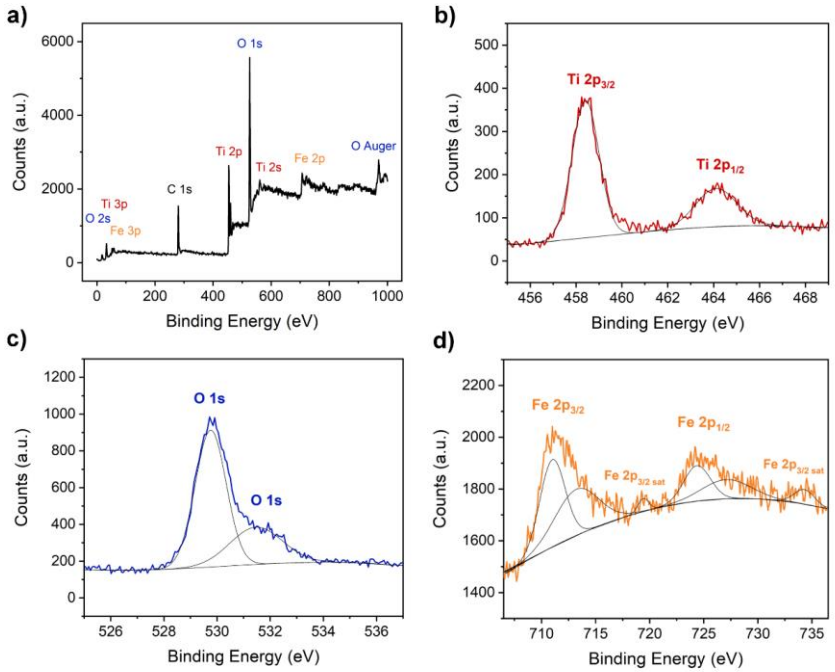

Figure 5 XPS spectra of hydrogenated titania nanorods with iron oxyhydroxide catalyst (H-TiO_2/FeOOH). (a) Survey. (b) Ti 2p. (c) O 1s. (d) Fe 2p.

The best results in terms of photoelectrochemical performances were obtained using a low concentrated solution (5 mM), resulting in a deposition charge of ~25 mC cm^{-2}. Catalyst loading was measured using ICP-OES on a 2 x 2 cm^2 sample area, ~1.64 μg cm^{-2} of FeOOH was measured. The catalyst improved significantly the photocurrent delivered at low overpotentials and shifted the onset potential, arbitrarily evaluated at 0.1 mA cm^{-2}, from 0.35 V vs RHE to 0.28 V vs RHE. On the other hand, at higher catalyst loading the maximum current delivered was reduced to 0.8 mA cm^{-2} while the same immersion potential under illumination and curve feature at low overpotential was maintained. A similar trend was found in the case of cobalt phosphate (Co-Pi) catalyst photoelectrodeposited onto a titania nanords array [17]. At high catalyst loading, the onset potential remained unchanged while the saturation current was reduced. To better visualize the effect of the FeOOH in the low-bias region, the anodic photoconversion

efficiency, measured considering only the half-cell, was defined using the following equation:

$$\eta = \frac{j_{ph}(E^0 - V)}{P_{light}}$$

Where j_{ph} [mA cm^{-2}] is the photocurrent density measured at the applied bias V [V], E^0 is the standard potential for the water electrolysis process (E^0=1.23 V) and P_{light} is the radiation power density (100 mW cm^{-2}).

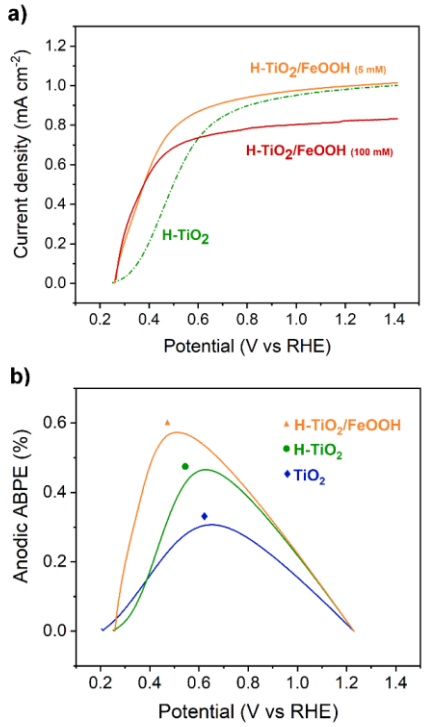

Figure 6 (a) Anodic linear sweep voltammetry of hydrogenated titania nanorods (H-TiO_2), with and without FeOOH catalyst, under AM 1.5 G illumination [100 mW cm^{-2}] in 1 M NaOH solution. 5 mM and 100 mM refer to the Fe^{3+} concentration in the photo-electrodeposition solution. (b) Anodic half-cell applied-bias photoconversion efficiency of TiO_2, H-TiO_2, and H-TiO_2/FeOOH photoelectrodes.

The presence of the catalysts on the surface reduced the recombination events of the photogenerated charges, as shown by the quenching of the photoluminescence observed (Fig 7a). This reduction could not be explained by a microstructure modification of the hydrogenated nanorods since the deposited catalyst is not expected to remove the trap sites introduced by the hydrogenation acting as recombination sites. This behavior may

Commentato [VR5]: È noto da letteratura? Ci vuole citazione nel caso. Oppure lo scriverei in modo più ipotetico

Commentato [GP6R5]: Abbiamo optato per rendere la frase più ipotetica

be correlated to the position of the electronic bands of the catalyst, slightly above the valence band of the hydrogenated TiO_2 [39,40]. So, the photogenerated holes in the hydrogenated TiO_2 were favored to be transferred in the catalyst layers. The charge transfer from the semiconductor surface to the electrolytic solution was studied through electrochemical impedance spectroscopy (EIS) to highlight the role of the FeOOH. The measurements were carried out under illumination, at the open circuit potential [18,41]. The Nyquist plot showed a significant reduction in the charge transfer resistance i.e. semicircle diameter, for the modified H-TiO_2 nanorods with respect to the bare one. This result demonstrates that the FeOOH improved the charge transfer, resulting in a higher photocurrent density at low bias.

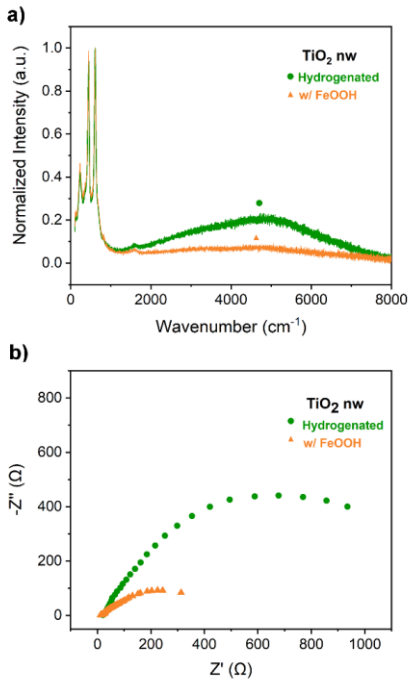

Figure 7 Effect of FeOOH catalyst on hydrogenated titania nanorods. (a) Photoluminescence spectrum. (b) Electrochemical impedance spectroscopy carried out at the open circuit potential, under AM 1.5 G illumination [100 mW cm^{-2}] in 1 M NaOH solution

The catalyst stability was evaluated through a 5 hours long test in which the photoelectrode surface potential was kept at + 1.23 V vs RHE, under constant illumination. Working under saturation conditions maximized the working current density, assessing the photostability in the worst scenario. The photocurrent density

stabilized at -1.05 mA cm^{-2} and remained constant for all the duration of the test, indicating that no secondary oxidation processes occurred. To confirm the integrity of the FeOOH catalyst, the photoelectrochemical behavior was analyzed right after the stability test. The LSV curve showed the same characteristic at low-bias, before reaching the saturation current density value, indicating the catalytic activity remained unchanged.

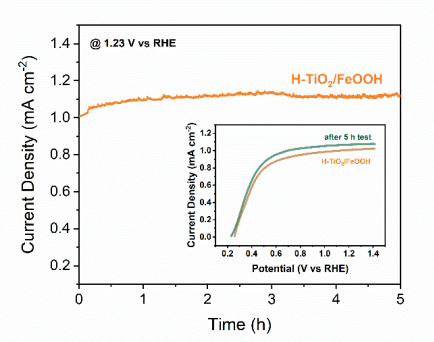

Figure 8 Stability test of the optimized H-TiO_2/FeOOH photoelectrode in 1 M NaOH solution at 1.23 V ss RHE, under AM 1.5 G illumination [100 mW cm-2]. Inset: anodic linear sweep voltammetry of the photoelectrode before and after the test.

4 Conclusions

In summary, we successfully implemented FeOOH onto hydrogenated TiO_2 nanorods array. The catalyst was deposited by a facile photo-electrodeposition method, based on earth-abundant elements and compatible with large area fabrication. The best performances were found at a catalyst loading of ~1.64 μg cm^{-2}, which resulted in an improved charge transfer and lower recombination. The H-TiO_2/FeOOH photoelectrode showed ~0.6 mA cm^{-2} at 0.4 V vs RHE, 1.4 times higher than the catalyst-free photoelectrodes, with a saturation current density of ~1.05 mA cm^{-2} at 1.23 V vs RHE. The improved photoelectrochemical behavior was maintained also after a 5 h test under constant illumination (1 sun) at 1.23 V vs RHE, in 1 M NaOH solution.

References

[1] A. Fujishima, K. Honda, Electrochemical photolysis of water at a semiconductor electrode, Nature. 238 (1972) 37–38. doi:10.1038/238037a0.

[2] K. Shankar, J.I. Basham, N.K. Allam, O.K. Varghese, G.K. Mor, X. Feng, M. Paulose, J.A. Seabold, K.S. Choi, C.A. Grimes, Recent advances In the use of TiO 2 nanotube and nanowire arrays for oxidative photoelectrochemistry, J. Phys. Chem. C. 113 (2009) 6327–6359. doi:10.1021/jp809385x.

[3] Y. Xie, Photoelectrochemical application of nanotubular titania photoanode, Electrochim. Acta. 51 (2006) 3399–3406. doi:10.1016/j.electacta.2005.10.003.

[4] G. Liu, L. Wang, H.G. Yang, H.M. Cheng, G.Q. Lu, Titania-based photocatalysts - Crystal growth, doping and heterostructuring, J. Mater. Chem. 20 (2010) 831–843. doi:10.1039/b909930a.

[5] A.Y.C. Tong, R. Braund, D.S. Warren, B.M. Peake, TiO 2-assisted photodegradation of pharmaceuticals - A review, Cent. Eur. J. Chem. 10 (2012) 989–1027. doi:10.2478/s11532-012-0049-7.

[6] U.I. Gaya, A.H. Abdullah, Heterogeneous photocatalytic degradation of organic contaminants over titanium dioxide: A review of fundamentals, progress and problems, J. Photochem. Photobiol. C Photochem. Rev. 9 (2008) 1–12. doi:10.1016/j.jphotochemrev.2007.12.003.

[7] D. Kang, T.W. Kim, S.R. Kubota, A.C. Cardiel, H.G. Cha, K.S. Choi, Electrochemical Synthesis of Photoelectrodes and Catalysts for Use in Solar Water Splitting, Chem. Rev. 115 (2015) 12839–12887. doi:10.1021/acs.chemrev.5b00498.

[8] J. Su, L. Vayssieres, A Place in the Sun for Artificial Photosynthesis?, ACS Energy Lett. 1 (2016) 121–135. doi:10.1021/acsenergylett.6b00059.

[9] C.X. Kronawitter, L. Vayssieres, S. Shen, L. Guo, D.A. Wheeler, J.Z. Zhang, B.R. Antoun, S.S. Mao, A perspective on solar-driven water splitting with all-oxide hetero-nanostructures, Energy Environ. Sci. 4 (2011) 3889–3899. doi:10.1039/c1ee02186a.

[10] B. Liu, E.S. Aydil, Growth of oriented single-crystalline rutile TiO 2 nanorods on transparent conducting substrates for dye-sensitized solar cells, J. Am. Chem. Soc. 131 (2009) 3985–3990. doi:10.1021/ja8078972.

[11] S. Tanemura, L. Miao, P. Jin, K. Kaneko, A. Terai, N. Nabatova-Gabain, Optical properties of polycrystalline and epitaxial anatase and rutile TiO 2 thin films by rf magnetron sputtering, in: Appl. Surf. Sci., Elsevier, 2003: pp. 654–660. doi:10.1016/S0169-4332(03)00015-1.

[12] Q. Meng, T. Wang, E. Liu, X. Ma, Q. Ge, J. Gong, Understanding electronic and optical properties of anatase TiO2 photocatalysts co-doped with nitrogen and transition metals, Phys. Chem. Chem. Phys. 15 (2013) 9549–9561. doi:10.1039/c3cp51476e.

[13] T. Leshuk, R. Parviz, P. Everett, H. Krishnakumar, R.A. Varin, F. Gu, Photocatalytic activity of hydrogenated TiO2, ACS Appl. Mater. Interfaces. 5 (2013) 1892–1895. doi:10.1021/am302903n.

[14] X. Yu, B. Kim, Y.K. Kim, Highly enhanced photoactivity of anatase TiO2 nanocrystals by controlled hydrogenation-induced surface defects, ACS Catal. 3 (2013) 2479–2486. doi:10.1021/cs4005776.

[15] G. Wang, H. Wang, Y. Ling, Y. Tang, X. Yang, R.C. Fitzmorris, C. Wang, J.Z. Zhang, Y. Li, Hydrogen-treated TiO2 nanowire arrays for photoelectrochemical water splitting, Nano Lett. 11 (2011) 3026–3033. doi:10.1021/nl201766h.

[16] I. Roger, M.A. Shipman, M.D. Symes, Earth-abundant catalysts for electrochemical and photoelectrochemical water splitting, Nat. Rev. Chem. 1 (2017) 1–13. doi:10.1038/s41570-016-0003.

[17] G. Ai, R. Mo, H. Li, J. Zhong, Cobalt phosphate modified TiO2 nanowire arrays as co-catalysts for solar water splitting, Nanoscale. 7 (2015) 6722–6728. doi:10.1039/c5nr00863h.

[18] Y. Pi, Z. Li, D. Xu, J. Liu, Y. Li, F. Zhang, G. Zhang, W. Peng, X. Fan, 1T-Phase MoS2 Nanosheets on TiO2 Nanorod Arrays: 3D Photoanode with Extraordinary Catalytic Performance, ACS Sustain. Chem. Eng. 5 (2017) 5175–5182. doi:10.1021/acssuschemeng.7b00518.

[19] W.M.A. El Rouby, M. Antuch, S.M. You, P. Beaunier, P. Millet, Novel nano-architectured water splitting photoanodes based on TiO2-nanorod mats surface sensitized by ZIF-67 coatings, Int. J. Hydrogen Energy. 44 (2019) 30949–30964. doi:10.1016/j.ijhydene.2019.08.220.

[20] H. Lin, L. Zhao, Novel g-C3N4/TiO2 nanorods with enhanced photocatalytic activity for water treatment and H2 production, J. Mater. Sci. Mater. Electron. 30 (2019) 18191–18199. doi:10.1007/s10854-019-02173-4.

[21] D.E. Schipper, Z. Zhao, A.P. Leitner, L. Xie, F. Qin, M.K. Alam, S. Chen, D. Wang, Z. Ren, Z. Wang, J. Bao, K.H. Whitmire, A TiO2/FeMnP Core/Shell Nanorod Array Photoanode for Efficient Photoelectrochemical Oxygen Evolution, ACS Nano. 11 (2017) 4051–4059. doi:10.1021/acsnano.7b00704.

[22] P. Yilmaz, A.M. Lacerda, I. Larrosa, S. Dunn, Photoelectrocatalysis of Rhodamine B and Solar Hydrogen Production by TiO2 and Pd/TiO2 Catalyst Systems, Electrochim. Acta. 231 (2017) 641–649. doi:10.1016/j.electacta.2017.02.035.

[23] J.A. Seabold, K.S. Choi, Efficient and stable photo-oxidation of water by a bismuth vanadate photoanode coupled with an iron oxyhydroxide oxygen evolution catalyst, J. Am. Chem. Soc. 134 (2012) 2186–2192. doi:10.1021/ja209001d.

[24] T.W. Kim, K.S. Choi, Nanoporous BiVO4 photoanodes with dual-layer oxygen evolution catalysts for solar water splitting, Science (80-.). 343 (2014) 990–994. doi:10.1126/science.1246913.

[25] J. Xiao, L. Fan, Z. Huang, J. Zhong, F. Zhao, K. Xu, S.F. Zhou, G. Zhan, Functional principle of the synergistic effect of co-loaded Co-Pi and FeOOH on Fe2O3 photoanodes for photoelectrochemical water oxidation, Chinese J. Catal. 41 (2020) 1761–1771.

doi:10.1016/S1872-2067(20)63618-X.

[26] C. Feng, S. Fu, W. Wang, Y. Zhang, Y. Bi, High-crystalline and high-aspect-ratio hematite nanotube photoanode for efficient solar water splitting, Appl. Catal. B Environ. 257 (2019) 117900. doi:10.1016/j.apcatb.2019.117900.

[27] R. Subbaraman, D. Tripkovic, K.C. Chang, D. Strmcnik, A.P. Paulikas, P. Hirunsit, M. Chan, J. Greeley, V. Stamenkovic, N.M. Markovic, Trends in activity for the water electrolyser reactions on 3d M(Ni,Co,Fe,Mn) hydr(oxy)oxide catalysts, Nat. Mater. 11 (2012) 550–557. doi:10.1038/nmat3313.

[28] M.S. Prévot, K. Sivula, Photoelectrochemical tandem cells for solar water splitting, J. Phys. Chem. C. 117 (2013) 17879–17893. doi:10.1021/jp405291g.

[29] H. Zhang, H. Wang, J. Xuan, Rational design of photoelectrochemical cells towards bias-free water splitting: Thermodynamic and kinetic insights, J. Power Sources. 462 (2020) 228113. doi:10.1016/j.jpowsour.2020.228113.

[30] Y. Chen, X. Feng, Y. Liu, X. Guan, C. Burda, L. Guo, Metal Oxide-Based Tandem Cells for Self-Biased Photoelectrochemical Water Splitting, ACS Energy Lett. 5 (2020) 844–866. doi:10.1021/acsenergylett.9b02620.

[31] A. Li Bassi, D. Cattaneo, V. Russo, C.E. Bottani, E. Barborini, T. Mazza, P. Piseri, P. Milani, F.O. Ernst, K. Wegner, S.E. Pratsinis, Raman spectroscopy characterization of titania nanoparticles produced by flame pyrolysis: The influence of size and stoichiometry, J. Appl. Phys. 98 (2005) 074305. doi:10.1063/1.2061894.

[32] L. Mascaretti, V. Russo, G. Zoppellaro, A. Lucotti, C.S. Casari, Š. Kment, A. Naldoni, A. Li Bassi, Excitation Wavelength- and Medium-Dependent Photoluminescence of Reduced Nanostructured TiO2 Films, J. Phys. Chem. C. 123 (2019) 11292–11303. doi:10.1021/acs.jpcc.9b01727.

[33] S. Gatto, M. Sansotera, F. Persico, M. Gola, C. Pirola, W. Panzeri, W. Navarrini, C.L. Bianchi, Surface fluorination on TiO2 catalyst induced by photodegradation of perfluorooctanoic acid, Catal. Today. 241 (2015) 8–14. doi:10.1016/j.cattod.2014.04.031.

[34] A.M. Beccaria, G. Poggi, G. Castello, Influence of passive film composition and sea water pressure on resistance to localised corrosion of some stainless steels in sea water, Br. Corros. J. 30 (1995) 283–287. doi:10.1179/bcj.1995.30.4.283.

[35] T.L. Barr, An ESCA study of the termination of the passivation of elemental metals, J. Phys. Chem. 82 (1978) 1801–1810. doi:10.1021/j100505a006.

[36] D. Brion, Etude par spectroscopie de photoelectrons de la degradation superficielle de FeS2, CuFeS2, ZnS et PbS a l'air et dans l'eau, Appl. Surf. Sci. 5 (1980) 133–152. doi:10.1016/0378-5963(80)90148-8.

[37] B. Zhang, X. Huang, Y. Zhang, G. Lu, L. Chou, Y. Bi, Unveiling the Activity and

Stability Origin of BiVO4 Photoanodes with FeNi Oxyhydroxides for Oxygen Evolution, Angew. Chemie - Int. Ed. 59 (2020) 18990–18995. doi:10.1002/anie.202008198.

[38] X. Yin, Q. Liu, Y. Yang, Y. Liu, K. Wang, Y. Li, D. Li, X. Qiu, W. Li, J. Li, An efficient tandem photoelectrochemical cell composed of FeOOH/TiO 2 /BiVO 4 and Cu 2 O for self-driven solar water splitting, Int. J. Hydrogen Energy. 44 (2019) 594–604. doi:10.1016/j.ijhydene.2018.11.032.

[39] A.A. Jelle, M. Hmadeh, P.G. O'Brien, D.D. Perovic, G.A. Ozin, Photocatalytic Properties of All Four Polymorphs of Nanostructured Iron Oxyhydroxides, ChemNanoMat. 2 (2016) 1047–1054. doi:10.1002/cnma.201600251.

[40] A. Shoneye, J. Tang, Highly dispersed FeOOH to enhance photocatalytic activity of TiO2 for complete mineralisation of herbicides, Appl. Surf. Sci. 511 (2020) 145479. doi:10.1016/j.apsusc.2020.145479.

[41] W. Han, L. Ren, L. Gong, X. Qi, Y. Liu, L. Yang, X. Wei, J. Zhong, Self-assembled three-dimensional graphene-based aerogel with embedded multifarious functional nanoparticles and its excellent photoelectrochemical activities, ACS Sustain. Chem. Eng. 2 (2014) 741–748. doi:10.1021/sc400417u.